 doi:10.20944/preprints202111.0269.v1

# Lead Solubility in the Kırklareli Stream, Turkey

Sultan Kıymaz [a], Hacer Gülocak [b], William F. Bleam[c]

[a]Land and Water Resources, University of Kırşehir Ahi Evran, Kırşehir, TURKEY
[b]Atatürk Soil and Water Agricultural Meteorology Research Institute, Kırklareli, TURKEY
[c]Department of Soil Science, University of Wisconsin-Madison, Madison, WI 53706, USA

Corresponding author: Sultan Kıymaz (Email address: skiymaz@ahievran.edu.tr)

## Abstract

The research was conducted in the Kırklareli stream, which flows southwest through the city of the same name toward the village of Kavaklı. The aim of the study is to evaluate water analysis results and assess the potential that the European Union drinking water standard for lead can be achieved in the Kırklareli stream by reliance on the low solubility of lead phosphate minerals. The present study used Visual MINTEQ 3.1 for all water chemistry simulations. The European Union drinking water standard for lead, which is 10 $\mu g\ L^{-1}$, is exceeded at least once and as many as three times at seven of the ten sites during the 2018 sampling season. Although the database solubility of hydroxypyromorphite is exceeded in most samples, it appears this may be the result of major ion substitutions in the hydroxypromorphite that forms in the Kırklareli stream which increases the effective solubility of lead in the stream.

KEYWORDS: Groundwater Chemistry, Surface Water Chemistry, Lead Toxicity, Lead Exposure, Solubility Diagrams, Solubility Modeling

*Preprint submitted to preprints.org*

## 1 Introduction

Ma et al. [1, 2], Ruby et al. [3], and Xu and Schwartz ([4]) were among the first to show lead phosphates could immobilize lead and other toxic trace elements in soils or sediments. The proposed mechanisms involve the co-precipitation of ions such as $Pb^{2+}$ with apatite group minerals and ion adsorption at surfaces of these minerals. Ma et al. [1, 2] and Šupová [5] document a broad range of cations and anions that replace calcium and phosphate in hydroxyapatite.

The E3/6, MINTEQA2, PHREEQC, Wateq4F and other databases include the solubility constant for tsumebite, a lead phosphate mineral not mentioned by Lindsay [6], Ma et al. [1, 2], Ruby et al. [3], and others who examined the chemistry of lead phosphate minerals. The tsumebite solubility constant appearing all major water chemistry databases was taken from Nriagu [7] who computed the solubility using the oxide-mixing method of Nriagu and Dell [8] for the composition $Pb_2Cu(PO_4)(OH)_3 \cdot 3\,H_2O(s)$. Crystallographic studies of tsumebite [9, 10] suggest sulfate replaces two of the hydroxyl ions yielding the composition $Pb_2Cu(PO_4)(SO_4)(OH) \cdot 3\,H_2O(s)$.

This study evaluates water analysis results by Gülocak [11] to determine whether reliance on the low solubility of these lead phosphate minerals is sufficient to meet lead drinking water standards for the European Union EU [12] and the Republic of Turkey [13] in Kırklareli stream.

## 2 Methods and Materials

### *2.1 Kırklareli Stream Study Site*

The thesis research by Gülocak [11] was conducted in the Kırklareli stream, which flows through the city of the same name. The water analysis data collected in this study was of a uniformly high quality and presented the opportunity to evaluate the possibility the low solubility of lead phosphate in a field setting could achieve the 10 $\mu g\ L^{-1}$ European Union drinking water standard for lead ([12]).

### *2.2 Water Sample Collection*

A full account of locations and dates when samples were collected can be found in Gülocak [11]. Briefly, Gülocak [11] collected water samples from ten sites (Figure 1) on Kırklareli stream from the southern outskirts of the city of Kırklareli to the village of Kavaklı, representing a distance of about 7.5

Preprints (www.preprints.org) | NOT PEER-REVIEWED | Posted: 15 November 2021 doi:10.20944/preprints202111.0269.v1

km. Water samples were collected throughout 2018, in winter (February), spring (March–April-May), summer (June-July) and autumn (October).

### *2.3 Sample Analysis*

A full account of sample analysis can be found in the thesis by Gülocak [11]. Briefly, water samples collected in one-liter bottles were analyzed for pH, temperature and electrical conductivity (EC) in the field and the water samples were stored in a refrigerator at 4°C until analysis.

Laboratory chemical analysis determined the dissolved concentration of the following ions: sodium (Na), calcium (Ca), magnesium (Mg), potassium (K), carbonate, bicarbonates, chloride (Cl), sulfate ($SO_4$), orthophosphate ($PO_4$), and a selection of trace elements: cadmium (Cd), cobalt (Co), copper (Cu), lead (Pb), zinc (Zn), floride (F), and nickel (Ni). Atatürk Research Institute of Soil, Water and Agricultural Meteorology in Kırklareli [14] performed both Inductively Coupled Plasma-Optical Emission Spectroscopy (ICP-OES) and ion chromatography analysis.

### *2.4 Water Chemistry Simulation*

We used Visual MINTEQ 3.0 [15] for all water chemistry simulations, basing all simulations on water chemistry analyses previously published in the thesis of Gülocak [11]. The water analysis pH values were verified by plotting water analysis calcium and alkalinity on calcite solubility diagrams and selecting a single $CO_2$(aq) concentration representative of the 2018 sampling season (February-July).

## 3 Results

### *3.1 Reliability of Water Analysis pH*

Several water chemists (e.g., [6, 16]) and others promote a method for water chemistry analysis that plots total solute concentrations on mineral solubility diagrams. This approach is most successful when the free ion activity are close to the total concentration measured by water analysis. In this study, we use this technique to verify the reliability of water analysis pH.

The calcite solubility diagram for Kırklareli stream (Figure 2) plots the base-10 logarithm of the total dissolved calcium to alkalinity moles-of-charge ratio and the base-10 logarithm of the total dissolved calcium molar concentration. There is considerable scatter of the data points but there is a clear alignment of the data with the linear relationship between the variables

Preprints (www.preprints.org) | NOT PEER-REVIEWED | Posted: 15 November 2021 doi:10.20944/preprints202111.0269.v1


Figure 1: Sample stations on Kırklareli stream. The top of the map is inclined 57°to the west of true north.

Preprints (www.preprints.org) | NOT PEER-REVIEWED | Posted: 15 November 2021 doi:10.20944/preprints202111.0269.v1

imposed by calcite solubility. The effective $CO_2(aq)$ concentration representative of the 2018 sampling season (Figure 2, dashed line) is $1.4 \cdot 10^{-3}$ *molar*.

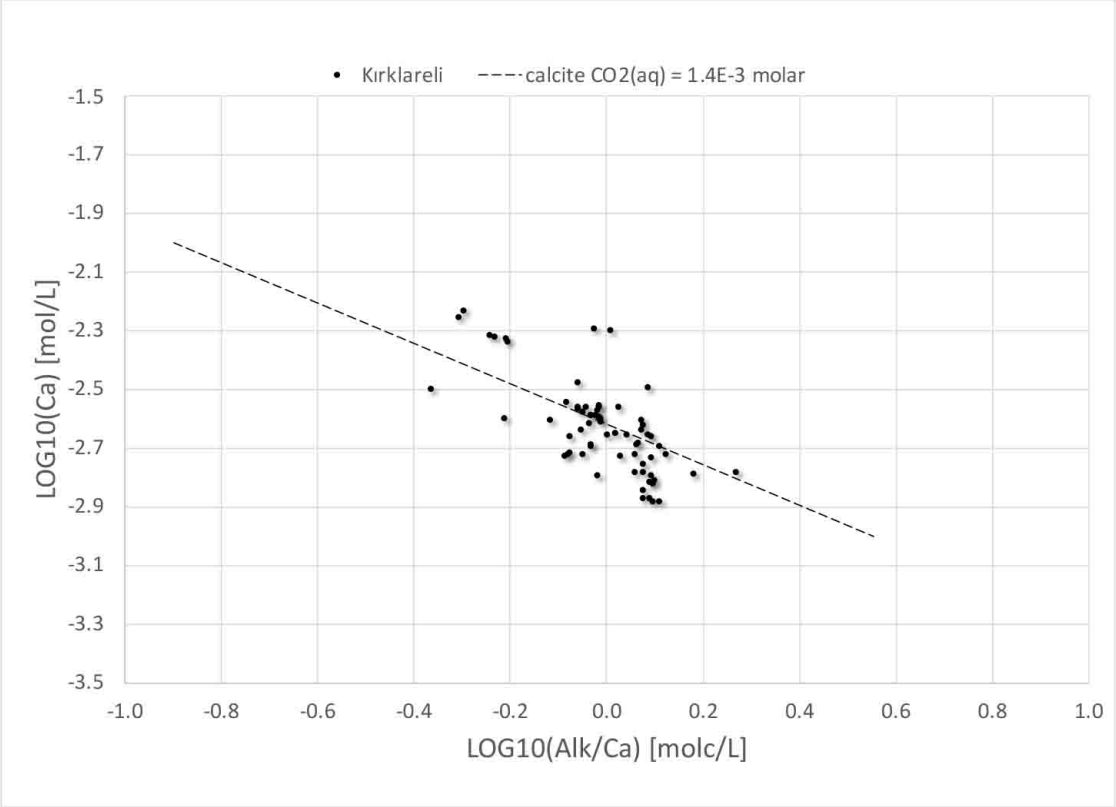


Figure 2: Calcite solubility in the Kırklareli stream (Turkey). The data points are based on total dissolved calcium and alkalinity. The dashed line plots calcite solubility using $Ca^{2+}$ and $HCO_3^-$ activity, respectively, and a $CO_2(aq)$ concentration of $1.4 \cdot 10^{-3}$ *molar*.

MINTEQA2 simulations using this representative $CO_2(aq)$ concentration agreed with the water analysis pH values reported by Gülocak ([11]) to within 0.2 of a pH unit. Subsequent MINTEQA2 simulations used a $CO_2(aq)$ concentration of $1.4 \cdot 10^{-3}$ *molar*.

### *3.1.1 Saturation Index Assessment*

Every MINTEQA2 simulation listed the ion activity products and saturation indexes for all minerals in the database with solubility expressions matching the basis ions and ion species from the water analyses. Review of

Preprints (www.preprints.org) | NOT PEER-REVIEWED | Posted: 15 November 2021 doi:10.20944/preprints202111.0269.v1

this output revealed numerous instances of oversaturation of hydroxyapatite, fluorapatite, hydroxypyromorphite, fluoropyromorphite, and tsumebite. These results prompted us to evaluate more carefully the implications for EU lead drinking water standards.

### *3.2 Solubility of Phosphate Minerals*

Lindsay and Moreno [17] plotted fluorapatite solubility assuming $F^-$ concentrations were controlled by fluorite solubility with a constant $Ca^{2+}$ activity of $5 \cdot 10^{-3}$. Zhang et al. [18] plotted fluorapatite solubility diagrams "calculated according to the determination of the soil solution," i.e., $Ca^{2+}$ activity of $3.16 \cdot 10^{-3}$ and $F^-$ of $2 \cdot 10^{-3}$. The solubility of fluorapatite (Figure 3 and Figure 5) and fluoropyromorphite (Figure 4 and Figure 6) are plotted using the same approach as Zhang et al. [18].

Fluorine concentrations in the Kırklareli stream during the 2018 sampling season varied little: $5 \pm 5 \cdot 10^{-5}$ *molar*. All fluorapatite and fluoropyromorphite solubility lines appearing in figures Figure 3 to Figure 6 were plotted assuming a $F^-$ activity of $5 \cdot 10^{-5}$.

Applying the same method as Nriagu [7], we computed the Standard Free Energy of Formation for a (sulfato)tsumebite with the composition suggested by Nichols [9] and Frost [10] $Pb_2Cu(PO_4)(SO_4)OH\,H_2O\,(s)$. Complete details of our estimate appear in the Appendix accompanying this paper.

Figure 4 and Figure 6 plot the solubility of three minerals: tsumebite, hydroxypyromorphite and fluoropyromorphite. The predicted solubility of (sulfato)tsumebite is much lower than phosphatotsumebite and was not plotted in the lead phosphate solubility diagrams.

### *3.3 Calcium-Phosphate Solubility Diagram: Water Analysis Values*

Figure 3 plots water analysis data from the Kırklareli stream (total dissolved calcium and orthophosphate) and the solubility lines for hydroxyapatite and fluorapatite. The mean dissolved fluoride concentration in Kırklareli stream results in a fluorapatite solubility that is indistinguishable from hydroxyapatite solubility.

The data points indicate a consistent over-saturation of hydroxyapatite-fluorapatite in Kırklareli stream, consistent with the saturation index results from our MINTEQA2 simulations. Typically, results such as those appearing in Figure 3 suggest persistent disequilibrium with a trend toward saturation as hydroxyapatite-fluorapatite precipitate.

Preprints (www.preprints.org) | NOT PEER-REVIEWED | Posted: 15 November 2021 doi:10.20944/preprints202111.0269.v1

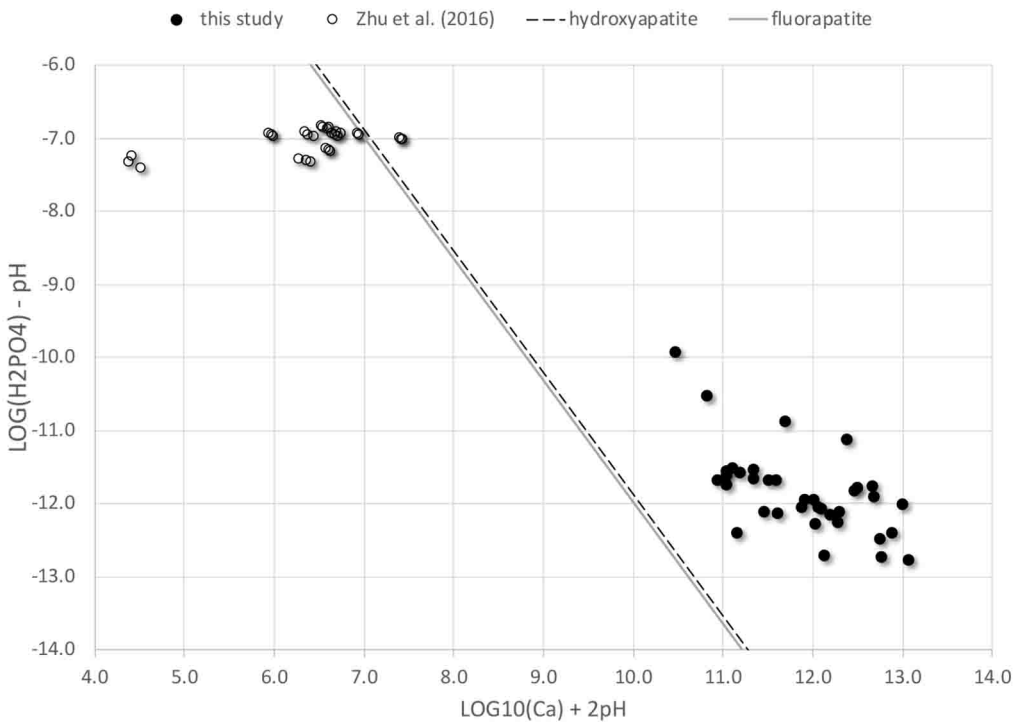


Figure 3: Calcium phosphate solubility in the Kırklareli stream (Turkey). The data points are based on total dissolved calcium, total dissolved phosphate and water analysis pH. The fluorapatite solubility line is plotted based the mean total dissolved fluoride ($5{\cdot}10^{-5}$ *molar*) in the Kırklareli stream during the 2018 sampling season. Data from Zhu et al. [19] are included (open circles) for reference.

Preprints (www.preprints.org) | NOT PEER-REVIEWED | Posted: 15 November 2021 doi:10.20944/preprints202111.0269.v1

### *3.4 Lead-Phosphate Solubility Diagram: Water Analysis Values*

Unlike the calcium phosphate minerals appearing in Figure 3, the solubility of fluoropyromorphite plots higher than the solubility of hydroxypyromorphite (Figure 4). The water analysis data are vastly over saturated relative to tsumebite $Pb_2Cu(PO_4)(OH)_3\,H_2O\,(s)(s)$ and (sulfato)tsumebite $Pb_2Cu(PO_4)(SO_4)OH\,H_2O\,(s)$ (not shown).

Regardless of the inclusion of (sulfato)tsumebite in the major water chemistry databases, the results in Figure 4 suggest conditions suitable for tsumebite precipitation for aqueous solution do not exist in Kırklareli stream, its sediments, or the soils whose drainage water recharge the stream.

As in Figure 3, when data points representing total dissolved lead and phosphate are plotted there is significant scatter. The distribution of data points in Figure 4 suggests dissolved lead and phosphate range from under saturation to somewhat over saturated relative to the less soluble hydroxypyromorphite and consistently under saturation relative to fluoropyromorphite.

### *3.5 Calcium-Phosphate Solubility Diagram: Ion Activity Values*

Zhu et al. [19] used X-ray diffraction to confirm unit cell changes accompanying the complete $Pb^{2+}$ replacement of $Ca^{2+}$ in hydroxyapatite in a series of mixed calcium-lead minerals with the composition

$$(Pb_xCa_{1-x})_5(PO_4)_3OH(s)$$

where $0 \leq x \leq 1$. Zhu et al. [19] also measured the solubility of these substituted hydroxyapatite minerals and verified this substitution was an ideal mixture of these two cations.

$$(Pb_xCa_{1-x})_5(PO_4)_3\,OH\,(s) \longleftrightarrow$$
$$5x\,Pb^{2+}(aq) + (5\text{-}5\,x)\,Ca^{2+}(aq) + 3\,PO_4^{3-}(aq) + OH^-(aq)$$

The solubility reaction appears above. The equilibrium solubility constant $K_{s0}^{\circ}$ is given by expressions (1) and the Standard Free Energy of Reaction $\Delta_r G^{\circ}$ by expression (2).

$$K_{s0}^{\circ} = (a_{Pb^{2+}(aq)})^{5x} \cdot (a_{Ca^{2+}(aq)})^{5-5x} \cdot (a_{PO_4^{3-}(aq)})^3 \cdot a_{OH^-(aq)} \tag{1}$$

$$\Delta_r G^{\circ} = -R \cdot T \cdot ln K_{s0}^{\circ} \tag{2}$$

Preprints (www.preprints.org) | NOT PEER-REVIEWED | Posted: 15 November 2021 doi:10.20944/preprints202111.0269.v1

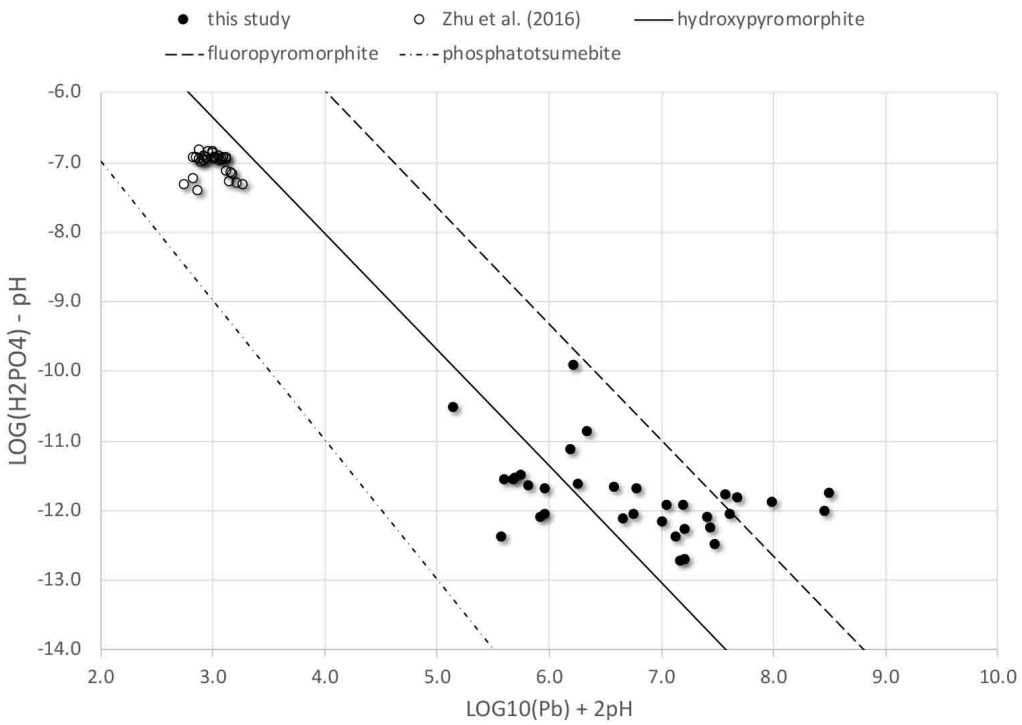


Figure 4: Lead phosphate solubility in the Kırklareli stream (Turkey). The data points are based on total dissolved lead, total dissolved phosphate and water analysis pH. The fluoropyromorphite solubility line is plotted based the mean total dissolved fluoride ($5 \cdot 10^{-5}$ *molar*) in the Kırklareli stream during the 2018 sampling season. Data from Zhu et al. [19] are included (open circles) for reference.

Preprints (www.preprints.org) | NOT PEER-REVIEWED | Posted: 15 November 2021 doi:10.20944/preprints202111.0269.v1

Based on expression (1) we would expect a curved solubility line for a series of substituted hydroxyapatite minerals, the curvature resulting from combining the solubility constant $K_{s0} = f(x)$ and the $Pb^{2+}(aq)$ ion activity into a variable intercept when plotting using the axis parameters in Figure 4 and Figure 6.

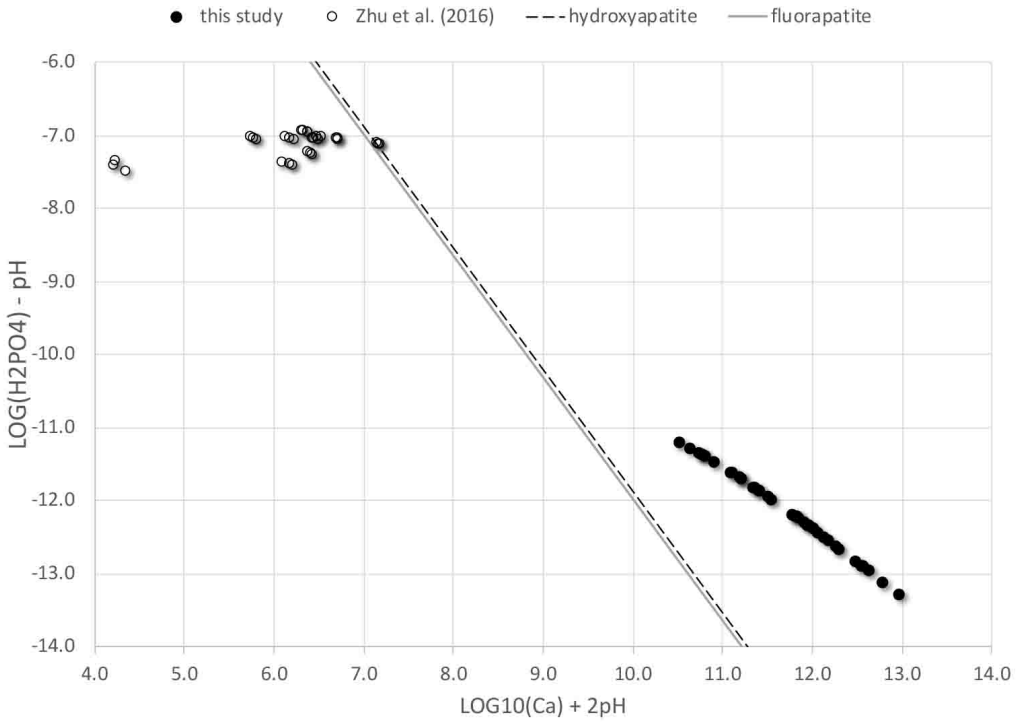


Figure 5: Calcium phosphate solubility in the Kırklareli stream (Turkey). The data points are based on simulated $Ca^{2+}(aq)$ and $H_2PO_4{}^-(aq)$ ion activities and water analysis pH. The fluorapatite solubility line is plotted based the mean activity of fluoride ($5 \cdot 10^{-5}$) in the Kırklareli stream during the 2018 sampling season. Data from Zhu et al. [19] are included (open circles) for reference.

The calcium-phosphate solubility data from Zhu et al. [19] appear in both figures Figure 3 and Figure 4. The Zhu et al. [19] data are slightly under saturated relative to the hydroxyapatite solubility constant appearing in MINTEQA2. The replacement of $Ca^{2+}$ in hydroxyapatite by $Pb^{2+}$ does not lead to a significant change in the slope of the Zhu et al. [19] data.

The data points appearing in Figure 5 are based on simulated $Ca^{2+}(aq)$

Preprints (www.preprints.org) | NOT PEER-REVIEWED | Posted: 15 November 2021 doi:10.20944/preprints202111.0269.v1

and $H_2PO_4^-$(aq) ion activities, not the total water analysis calcium and phosphate plotted in Figure 3. The data points in Figure 5 plot with little scatter along a slightly curved solubility line. This curvature would be consistent with a substituted hydroxyapatite which, given the dissolved lead concentrations in Kırklareli stream, cannot not be the result of a reaction such as that given by expression (1).

Data from Zhu et al. [19] represent the solubility effect of $Ca^{2+}$ replacement by $Pb^{2+}$ in a series of substituted, laboratory-prepared hydroxyapatite minerals. Our data from Kırklareli stream (Turkey) plots above the stoichiometric hydroxyapatite solubility line, trending to lower solubility, while the data from Zhu et al. [19] plot on and below the solubility line.

We suggest the results appearing in Figure 5 arise from some combination of major cations and anions substituting for both calcium and phosphate in the apatite that forms Kırklareli stream, leading to the higher solubility and the slight curvature of the ion activity data points. The emphasis here is on major cations and anions, not trace cations and anions.

### *3.6 Lead-Phosphate Solubility Diagram: Ion Activity Values*

The data points appearing in Figure 6 are based on simulated $Ca^{2+}$(aq) and $H_2PO_4^-$(aq) ion activities, not the total water analysis lead and phosphate plotted in Figure 4. The data points in Figure 6, as is the case in Figure 5, plot without scatter along a distinctly curved solubility line. This curvature would be consistent with a substituted hydroxypyromorphite which, given the dissolved lead concentrations in Kırklareli stream, could be the result of $Pb^{2+}$ replacement in hydroxypyromorphite by the major cation $Ca^{2+}$ as in the reaction given by expression (1).

Data from Zhu et al. [19] represent the solubility effect of $Pb^{2+}$(aq) replacement by $Ca^{2+}$(aq) in a series of substituted, laboratory-prepared hydroxypyromorphite minerals in the absence of alkalinity and calcite saturation. Our data from Kırklareli stream crosses the stoichiometric hydroxypyromorphite solubility line, trending to lower solubility, while the data from Zhu et al. [19], representing low alkalinity conditions, plot below the stoichiometric hydroxypyromorphite solubility line.

We suggest the lead-phosphate activity points appearing in Figure 6 arises from a similar non-stoichiometric effect as that described by Zhu et al. [19] for synthetic hydroxypyromorphites. Some combination of major cations replaces $Pb^{2+}$ in the pyromorphite that forms in Kırklareli stream leading to

Preprints (www.preprints.org) | NOT PEER-REVIEWED | Posted: 15 November 2021 doi:10.20944/preprints202111.0269.v1

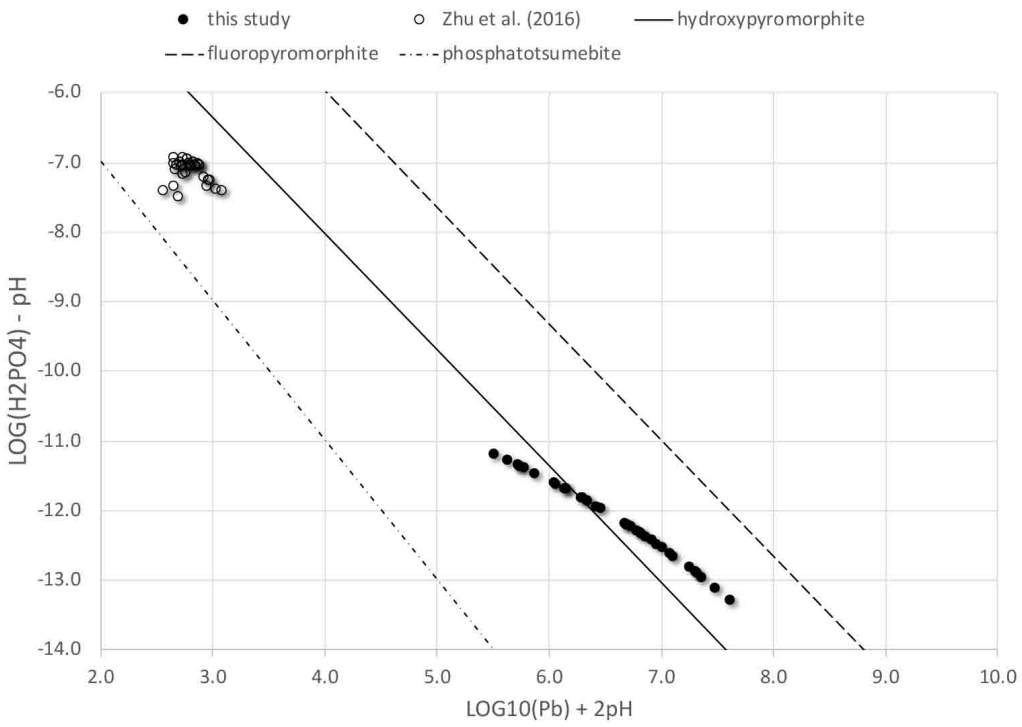


Figure 6: Lead phosphate solubility in the Kırklareli stream (Turkey). The data points are based on simulated $Pb^{2+}(aq)$ and $H_2PO_4^-(aq)$ ion activities and water analysis pH. The fluorapatite solubility line is plotted based the mean activity of fluoride ($5 \cdot 10^{-5}$) in the Kırklareli stream during the 2018 sampling season. Data from Zhu et al. [19] are included (open circles) for reference.

the higher solubility and slight curvature of the ion activity data points in Figure 6.

## 4 Discussion

The results in Figure 4 and Figure 6 suggest hydroxyapatite-fluorapatite and hydroxypyroporphite solubility in Kırklareli stream most likely results from major ion substitutions rather than disequilibrium involving hydroxyapatite-fluorapatite and hydroxypyroporphite minerals with ideal compositions. These substitutions result in a modest increase in the solubility of non-stoichiometric hydroxypyromorhite in Kırklareli stream.

We also propose the coupling of apatite mineral solubility to pyromorphite mineral solubility. A key consequence of this coupling of apatite mineral to pyromorphite mineral solubility, as noted above, is the substitution of the minor cation $Pb^{2+}$ in hydroxypyromorphite by the major cation $Ca^{2+}$.

We find no evidence that the highly insoluble mineral tsumebite forms either in the soils of the Kırklareli basin or the stream itself. While it is possible to imagine tsumebite precipitating from aqueous solution under surficial conditions, this does not appear to be likely based on our results.

## 5 Conclusion

In conclusion, there is clear evidence for the solubility coupling of pyromorphite-group mineral to apatite-group mineral in Kırklareli stream. This results from the natural stream chemistry, not from amendments added to groundwater or stream to alter lead solubility.

European Union and Republic of Turkey drinking water standards [12, 13] for lead ($10\ \mu g\ L^{-1}$) cannot be consistently achieved in Kırklareli stream through the natural solubility of the non-stoichiometric pyromorphite-group minerals that tend to form in this environment.

We recommend a survey of potable water sources, both wells and tributary streams, in the Kırklareli stream catchment for total dissolved lead. The collection of water sample should cover an annual cycle to determine whether water treatment to remove dissolved lead is needed to meet drinking water standards.

Preprints (www.preprints.org) | NOT PEER-REVIEWED | Posted: 15 November 2021 doi:10.20944/preprints202111.0269.v1

## 6 Acknowledgement

This study was based entirely from results appearing in the thesis of Hacer Gülocak [11].

## 7 Appendix

### *7.1 Thermodynamic Data*

MINTEQA2, and other water chemistry databases, include a solubility constant for the mineral $Pb_2Cu(PO_4)(OH)_3 \cdot 3\,H_2O\,(s)$ [20]. Using an oxide-mixing model [7], Nriagu [8] estimate the standard Gibbs energy of formation for this composition as: $\Delta_f G^{\circ} = -593.0\ kcal \cdot mol^{-1}$.

A later study of tsumebite by Nichols [9] proposed a different composition $Pb_2Cu(PO_4)(SO_4)OH \cdot 3\,H_2O\,(s)$ that was later confirmed in a chemical and vibrational spectroscopy study by Frost [10].

We used the oxide-mixing method of Nriagu [7, 8] to estimate the standard Gibbs energy of formation of a sulfato-tsumebite with the more recent composition $Pb_2Cu(PO_4)(SO_4)OH \cdot 3\,H_2O\,(s)$. Using the same thermodynamic data as Nriagu [7, 8, 21], the estimated standard Gibbs energy of formation of sulfato-tsumebite is $\Delta_f G^{\circ} = -594.2\ kcal \cdot mol^{-1}$.

Table 1: Thermodynamic data and sources

| Mineral | Source |
|---|---|
| $Pb_2Cu(PO_4)(OH)_3 \cdot 3\,H_2O\,(s)$ | [8] |
| $Pb_2Cu(PO_4)(SO_4)(OH) \cdot 3\,H_2O\,(s)$ | this work |
| $CuO\,(s)$ | [22] |

### *7.2 Tsumebite and Tenorite*

The reaction following gives the estimated solubility constant for tsumebite $Pb_2Cu(PO_4)(OH)_3 \cdot 3\,H_2O$ as listed in the first row of Table 1.

$$Pb_2Cu(PO_4)(OH)_3 \cdot 3\,H_2O\,(s) + 3\,H^+(aq) \xleftrightarrow{K_{s1}^{\circ} = 10^{-9.79}} 2\,Pb^{2+}(aq) + Cu^{2+}(aq) + PO_4^{3-}(aq) + 6\,H_2O\,(l)$$

Preprints (www.preprints.org) | NOT PEER-REVIEWED | Posted: 15 November 2021 doi:10.20944/preprints202111.0269.v1

The next reaction gives the estimated solubility constant for sulfato-tsumebite $Pb_2Cu(PO_4)(SO_4)(OH)\cdot 3\,H_2O$ [21] as listed in the second row of Table 1. The solubility constants for both forms of tsumebite are computed using the same thermodynamic data as Nriagu [7, 8, 21].

$$\begin{aligned} Pb_2Cu(PO_4)(SO_4)(OH)\cdot 3\,H_2O\,(s) + H^+(aq) \xleftrightarrow{K^{\circ}_{s1} = 10^{+2.33}} \\ 2\,Pb^{2+}(aq) + Cu^{2+}(aq) + PO_4^{3-}(aq) + SO_4^{2-}(aq) + 4\,H_2O\,(l) \end{aligned}$$

Finally, the solubility reaction and constant for tenorite $CuO\,(s)$ follows.

$$CuO\,(s) + 2\,H^+(aq) \xleftrightarrow{K^{\circ}_{s1} = 10^{+7.644}} Cu^{2+}(aq) + H_2O\,(l)$$

Combine the solubility reactions for tsumebite with tenorite to replace dissolved $Cu^{2+}(aq)$ with tenorite $CuO\,(s)$, yields a modified solubility reaction and constant for tsumebite.

$$\begin{aligned} Pb_2Cu(PO_4)(OH)_3\cdot 3\,H_2O\,(s) + H^+(aq) \xleftrightarrow{K^{\circ}_{s1} = 10^{-17.43}} \\ 2\,Pb^{2+}(aq) + CuO(s)) + PO_4^{3-}(aq) + 5\,H_2O\,(l) \end{aligned}$$

Similarly, combine the solubility reactions for sulfato-tsumebite with tenorite to replace dissolved $Cu^{2+}(aq)$ with tenorite $CuO\,(s)$, yields a modified solubility reaction and constant for sufato-tsumebite.

$$\begin{aligned} Pb_2Cu(PO_4)(SO_4)(OH)\cdot 3\,H_2O\,(s) \xleftrightarrow{K^{\circ}_{s1} = 10^{-5.13}} \\ 2\,Pb^{2+}(aq) + CuO(s)) + PO_4^{3-}(aq) + SO_4^{2-}(aq) + H^+(aq)\,3\,H_2O\,(l) \end{aligned}$$

The modified solubility reactions above effectively represent tsumebite and sulfato-tsumebite solubility, respectively, under conditions where $Cu^{2+}(aq)$ solubility is determined by tenorite $CuO\,(s)$.

Modifying solubility reactions so that they includes only the predominant species allows one to prepare a solubility diagram that plots both valid thermodynamic mineral solubility lines and empirical solution data based on total ion-analysis values.

To make this transformation, we need the following phosphate hydrolysis reaction.

$$H_2PO_4^-(aq) \xleftrightarrow{K^{\circ}_{a2} = 10^{-19.57}} PO_4^{3-}(aq) + 2\,H^+(aq)$$

Preprints (www.preprints.org) | NOT PEER-REVIEWED | Posted: 15 November 2021 doi:10.20944/preprints202111.0269.v1

When the phosphate hydrolysis reaction is combined with the tsumebite-tenorite solubility reaction, the overall tsumebite reaction appears below.

$$\mathrm{Pb_2Cu(PO_4)(OH)_3 \cdot 3\,H_2O\,(s) + 3\,H^+(aq) \xleftrightarrow{K^{\circ}_{s1} = 10^{-2.99}} 2\,Pb^{2+}(aq) + CuO\,(s) + H_2PO_4^-(aq) + 5\,H_2O\,(l)}$$

The logarithm of the equilibrium constant and quotient for the tsumebite-tenorite reaction is given by expressions (7.1) and (7.2).

$$2 \cdot \log_{10} \mathrm{Pb}^{2+} + \log_{10} \mathrm{H_2PO_4^-} - 3 \cdot \log_{10} \mathrm{H}^+ = -2.99$$

$$2 \cdot \log_{10} \mathrm{Pb}^{2+} + \log_{10} \mathrm{H_2PO_4^-} + 3 \cdot p\mathrm{H} = -2.99$$

$$2 \cdot \left(\log_{10} \mathrm{Pb}^{2+} + 2 \cdot p\mathrm{H}\right) + \left(\log_{10} \mathrm{H_2PO_4^-} - p\mathrm{H}\right) = -2.99$$

$$\left(\log_{10} \mathrm{H_2PO_4^-} - p\mathrm{H}\right) = -2 \cdot \left(\log_{10} \mathrm{Pb}^{2+} + 2 \cdot p\mathrm{H}\right) - 2.99 \qquad (7.1)$$

$$\left(p\mathrm{H_2PO_4^-} + p\mathrm{H}\right) = -2 \cdot \left(p\mathrm{Pb}^{2+} - 2 \cdot p\mathrm{H}\right) + 2.99 \qquad (7.2)$$

Similarly, when the phosphate hydrolysis reaction is combined with the sulfato-tsumebite-tenorite solubility reaction, the overall sulfato-tsumebite reaction appears below.

$$\mathrm{Pb_2Cu(PO_4)(SO_4)(OH) \cdot 3\,H_2O\,(s) + H^+(aq) \xleftrightarrow{K^{\circ}_{s1} = 10^{+9.13}} 2\,Pb^{2+}(aq) + CuO\,(s) + H_2PO_4^-(aq) + SO_4^{2-}(aq) + 3\,H_2O\,(l)}$$

The logarithm of the equilibrium constant and quotient for the sulfato-tsumebute reaction is given by expressions (7.3) and (7.4).

Preprints (www.preprints.org) | NOT PEER-REVIEWED | Posted: 15 November 2021 doi:10.20944/preprints202111.0269.v1

$$2 \cdot \log_{10} \mathrm{Pb}^{2+} + \log_{10} \mathrm{H_2PO_4^-} + \log_{10} \mathrm{SO_4^{2-}} - \log_{10} \mathrm{H}^{+} = +9.13$$

$$2 \cdot \log_{10} \mathrm{Pb}^{2+} + \log_{10} \mathrm{H_2PO_4^-} + \log_{10} \mathrm{SO_4^{2-}} + p\mathrm{H} = +9.13$$

$$2 \cdot \left(\log_{10} \mathrm{Pb}^{2+} + 2 \cdot p\mathrm{H}\right) + \left(\log_{10} \mathrm{H_2PO_4^-} - p\mathrm{H}\right) + \left(\log_{10} \mathrm{SO_4^{2-}} - 2 \cdot p\mathrm{H}\right) = +9.13$$

$$\left(\log_{10} \mathrm{H_2PO_4^-} - p\mathrm{H}\right) =$$

$$-2 \cdot \left(\log_{10} \mathrm{Pb}^{2+} + 2 \cdot p\mathrm{H}\right) - \left(\log_{10} \overline{\mathrm{SO_4^{2-}}} - 2 \cdot \overline{p\mathrm{H}} - 9.13\right) \quad (7.3)$$

$$\left(p\mathrm{H_2PO_4^-} + p\mathrm{H}\right) = -2 \cdot \left(p\mathrm{Pb}^{2+} - 2 \cdot p\mathrm{H}\right) - \left(\overline{p\mathrm{SO_4^{2-}}} + 2 \cdot \overline{p\mathrm{H}} + 9.13\right) \quad (7.4)$$

Expressions (7.3) and (7.4) use the *mean* $\mathrm{SO_4^{2-}}$(aq) concentration and mean $p$H value for the data set in exactly the same way as plots of fluorapatite and fluoropyromorphite solubility lines are plotted using the mean $\mathrm{F^-}$ concentration for the data set.

## References


[1] Q Y Ma et al. "*In situ* lead immobilization by apatite". In: *Environmental Science & Technology* 27.9 (1993), pp. 1803–1810.

[2] Q Y Ma, T J Logan, and S J Traina. "Lead immobilization from aqueous solutions and contaminated soils using phosphate rocks". In: *Environmental Science & Technology* 29.4 (1995), pp. 1118–1126.

[3] M V Ruby, A Davis, and A Nicholson. "*In situ* formation of lead phosphates in soils as a method to immobilize lead". In: *Environmental science & technology* 28.4 (1994), pp. 646–654.

[4] Y Xu and F W Schwartz. "Lead immobilization by hydroxyapatite in aqueous solutions". In: *Journal of Contaminant Hydrology* 15.3 (1994), pp. 187–206.

[5] M Šupová. "Substituted hydroxyapatites for biomedical applications: A review". In: *Ceramics international* 41.8 (2015), pp. 9203–9231.

[6] W L Lindsay. *Chemical equilibria in soils.* John Wiley and Sons Ltd., 1979.

[7] J O Nriagu. "Lead orthophosphates—IV Formation and stability in the environment". In: *Geochimica et Cosmochimica Acta* 38.6 (1974), pp. 887–898.

[8] J O Nriagu and C I Dell. "Diagenetic formation of iron phosphates in recent lake sediments". In: *American Mineralogist* 59.9-10 (1974), pp. 934–946.

[9] M C Nichols. "The structure of tsumebite". In: *American Mineralogist* 51.1-2 (1966), p. 267.

[10] R L Frost, S J Palmer, and Y Xi. "Raman spectroscopy of the multi anion mineral arsentsumebite Pb2Cu (AsO4)(SO4)(OH) and in comparison with tsumebite Pb2Cu (PO4)(SO4)(OH)". In: *Spectrochimica Acta Part A: Molecular and Biomolecular Spectroscopy* 83.1 (2011), pp. 449–452.

[11] H Gulocak. "Determination of the Usage of Wastewaters in Kırklareli Region for Irrigation in Agriculture [Translated Title]. Kırklareli Yoresindeki Atıksuların Tarımda Sulama Amaçlı Kullanılabilirliğinin Nelirlenmesi". Turkish. Masters of Science thesis. Kırşehir Ahi Evran Universitesi, 2018.

[12] European Communities. *European Communities (drinking water) (no. 2), Regulatıons. Statutory Instrument Number 278 of 2007*. 2007. URL: http://www.irishstatutebook.ie/eli/2007/si/278/made/en/print.

[13] Official Gazette of the Republic of Turkey [English Translation. *Regulation Amending the Regulation on Surface Water Quality Management. Issue 29327*. 2015. URL: https://www.resmigazete.gov.tr/eskiler/2015/04/20150415-18.pdf.

[14] L S Clesceri, A D Eaton, and A E Greenberg. *Standard Methods for the Examination of Water and Wastewater*. 20th. Washington, DC: American Public Health Association, American Water Works Association, Water Environment Federation, Water Pollution Control Federation, 1998.

[15] J D Allison, D S Brown, and K J Novo-Gradac. "MINTEQA2/PRODEFA2, A Geochemical Assessment Model for Environmental Systems: Version 3.0 User's Manual". In: (1991).

[16] R M Garrels and C L Christ. *Solutions, Minerals, and Equilibria.* Harper Row, 1965.

[17] W L Lindsay and E C Moreno. "Phosphate phase equilibria in soils". In: *Soil Science Society of America Journal* 24.3 (1960), pp. 177–182.

[18] M Zhang et al. "Phosphate minerals and solubility in native and agricultural calcareous soils". In: *Geoderma* 232 (2014), pp. 164–171.

[19] Yinian Zhu et al. "Characterization, dissolution and solubility of the hydroxypyromorphite–hydroxyapatite solid solution [(Pb x Ca 1- x) 5 (PO 4) 3 OH] at 25° C and pH 2–9". In: *Geochemical transactions* 17.1 (2016), pp. 1–18.

[20] L LaForge. "Crystallography of tsumebite". In: *American Mineralogist* 23.11 (1938), pp. 772–782.

[21] D D Wagman. *Selected Values of Chemical Thermodynamic Properties: Tables for the First Thirty-Four Elements in the Standard Order of Arrangement*. Vol. 270. 3. Department of Commerce, National Bureau of Standards, 1968.

[22] Virginia Herndon. "MINTEQA2/PRODEFA2, A Geochemical Assessment Model for Environmental Systems: User Manual Supplement for Version 4.0". In: (1998).